University of Crete
Department of Physics

Assessment of the localizability of Ultra-High Energy Cosmic-Ray (UHECR) sources through next-generation optopolarimetric experiments.

Master Thesis of
Velli Maria – Christina
Supervisor: Prof. Pavlidou Vasiliki

Greece,
February 2018

Contents

1 Abstract

The sources of the most energetic particles known in our universe (Ultra-High Energy Cosmic Rays), still remain unknown. Their discovery will not only enlighten the mystery of what mechanism (cosmic accelerator) could possibly accelerate these particles up to energies 10^{20} eV, but also will possibly reveal new particle physics, or new astrophysical objects.

The main reason why it is difficult to locate such sources is because particles coming from them are ionized atoms and so they get deflected by the Galactic magnetic field and our knowledge of its 3-dimensional structure is limited. That is because until today only observations of quantities integrated along the line of sight are possible. Next-generation optopolarimetric experiments such as the PASIPHAE programme, will provide such information in the near future and so we will be able to back-propagate/correct the trajectories of the highest-energy cosmic rays. In this work we examine how the significance of the detection of an UHECR source gets better with such correction.

Our results show that for a very plausible correction, such as reducing the deflection angles to half their current values, then for an initial 3σ significance reported source, we would get the significance to rise to 4.5σ.

2 Introduction

2.1 Background Knowledge

Cosmic rays are ionized atoms that impact the Earth's atmosphere, and produce showers of secondary particles that reach the surface. They originate outside of the solar system and most probably outside our galaxy. As UHECRs we define the cosmic rays with energies above 10^{18} eV, and observing them in such energies, raises a great number of questions:

- What are their sources and what is their distribution in space?
- What can we learn about the conditions that exist in these sources?
- Are the primaries (the ionized atom that firstly impacts the atmosphere) protons or heavier nuclei (Fe)?
- What is their acceleration mechanism?
- What knowledge can we gain in particle physics from energies that are far from accessible with terrestrial accelerators?
- How can we constrain the structure and strength of galactic and extragalactic magnetic fields that these CRs passed through?

In order to answer any of these questions we need to solve their intrinsic problem as charged particles: their deflection by the magnetic field, that is caused by the Lorentz force.

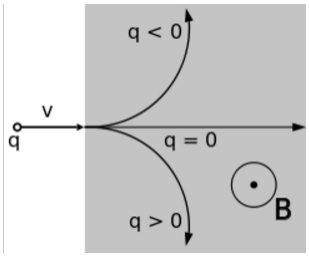

Figure 1a

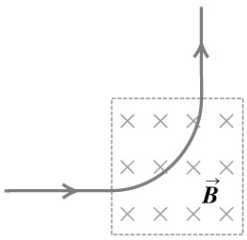

Figure 1b

When a particle of charge q is moving with velocity $\vec{v}$ in a magnetic field $\vec{B}$ then the Lorentz force is $\vec{F} = q\vec{v} \times \vec{B}$, and so the perpendicular to the motion component of $\vec{B}$, has the only contribution to the force, and in turn in the deflection.

The purpose is to back propagate their trajectories, but to do so we need to know the magnetic field, and we have very little knowledge of it. That is because we only have measurements integrated along the line of sight. In fact, any 3-dimensional information about it comes from models, and even the most recent best-constrained ones contain a large random component.

Here is where PASIPHAE comes in [1]. The PASIPHAE program will measure with extremely high accuracy the polarisation of approximately 10^6 stars at areas with galactic latitude such that the Galactic plane is avoided. This data will be combined with the distances of the stars obtained by the ESA's on-going Gaia mission. That way, it is possible to produce

the first Magnetic Tomography of our galaxy (3-dimensional structure of the magnetic field), which in turn will not only help with our case but also assist in numerous physical problems that face the problem of dust interference with their measurements (such as searching for B-modes), because then it will be possible to extract the dust component.

2.2 Energy Spectrum

The first spectrum we see is derived combining data from different experiments. The second one is explicitly from data from Pierre Auger observatory, where they follow a technique in which they consider their data to be in 4 independent data sets (depending on the inclination of the air shower, and the detector that recorded them) and then they statistically combine them.

As it can be seen in figure 2b, the flux at energies above $10^{19.5}$ eV drops for more than an order of magnitude. That cut-off is called the GZK (Greisen–Zatsepin–Kuzmin) cut-off. This is due to energy losses from photo-pion production when the cosmic rays interacts with the cosmic microwave background, and is an indication for extragalactic sources since cosmic rays need to have traveled several Mpc (10^6 parsec) in order to have such energy losses. There are also two other indications for extragalactic sources. First, if a cosmic ray with such energy was created in our Galaxy, due to the strength of the magnetic field, the gyroradius would be several kpc (10^3 parsec) and so it would immediately leave the Galaxy. Secondly, as we will see in section 2.4 there is a large scale anisotropy reported by the Pierre Auger Observatory, and the dipole representing it points 120 degrees from the Galactic center.

Two other characteristics of this spectrum are the so called knee and ankle, located around 10^{15} and 5×10^{18} eV respectively. The ankle is an indication for transition from galactic to extragalactic sources [2].

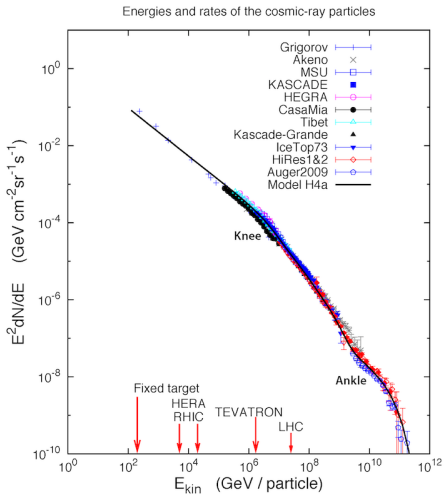

Figure 2a

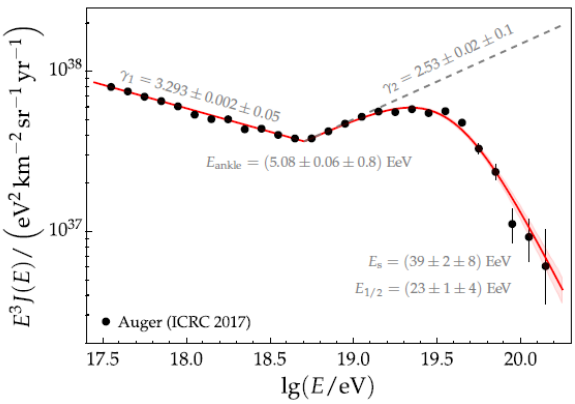

Figure 2b

2.3 Mass composition and atmospheric depth

The mass composition of UHECRs is not directly measured. Instead we study another parameter, the atmospheric depth Xmax. That is the altitude where we have the maximum number of particles in the air shower. If E is the energy of the primary and A is the nuclear mass number, the dependence is $\langle X_{max} \rangle \sim log(E/A)$, so we see that lighter primaries such as protons penetrate deeper into the atmosphere than heavy ones such as iron. It is important to know the UHECR composition, because related simulations strongly depend on that, and results differ a lot between protons and iron

In the plots that follow we see the atmospheric depth and its standard deviation for energies ranging from 10^{17} to 10^{20} eV. The red and blue lines refer to post LHC models (models that extrapolate the particle physics beyond LHC current operating energies (13 TeV)) for protons and iron respectively.

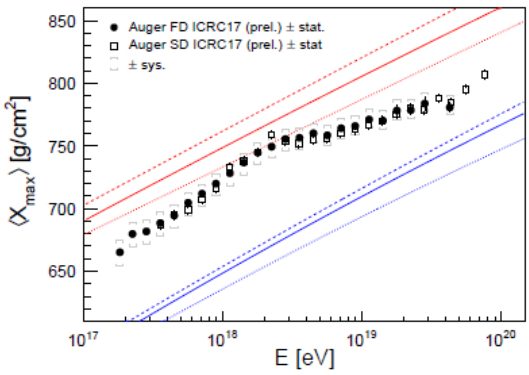

Figure 3a

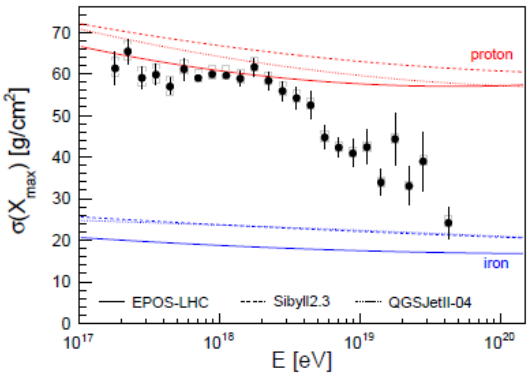

Figure 3b

In figure 3a we can see that $\langle X_{max} \rangle$ evolves with energy with a break at $10^{18.33 \pm 0.02}$ eV. Before the break, the average mass evolves towards a lighter composition since we have a higher slope that the theoretical ones shown in blue and red lines. After the break the trend is reversed and the average mass decreases with energy. The break is an indication for a transition from a heavy Galactic, to a light extragalactic composition [2].

In figure 3b we have the standard deviation of X_{max}. Bigger values of sigma come from either light or mixed composition, and so for example the value of the atmospheric depth fluctuates more for protons. At high energies there is a clear indication of a more pure and heavy composition [2].

2.4 Anisotropies in sky distribution

It is important that we see that anisotropies exist in the sky maps because it is an indication for lighter composition since iron deflects a lot more. Furthermore, if the cosmic rays are already clustering despite being deflected, then this effect will be much enhanced after a possible back propagation, and that will help us know where to look for sources.

In the plots below we can see the sky maps of these anisotropies from the Pierre Auger Observatory, and the Telescope Array respectively. The first map is in galactic coordinates (l, b) and the dipole points at (233, -13) degrees [2]. The second one is in equatorial coordinates

(R.A., dec) and the hot spot is at (146.7, 43.2) degrees [3]. These 2 directions may be at odds, but the Telescope Array cannot see the spot the Pierre Auger Observatory reports since Auger is in the South (Argentina) while Telescope Array is in the North (Utah, U.S.). Specifically, galactic coordinates (233, -13) translate to (100,-23) equatorial and the limit of telescope array is at declination -10 degrees.

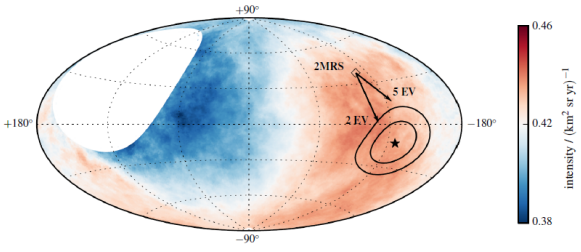

Figure 4a

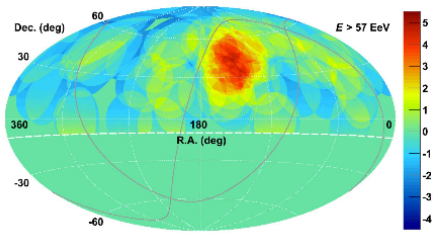

Figure 4b

2.5 Gamma Ray Astronomy

Gamma ray sources are an excellent example of sources with small flux of photons over a high-intensity background. They have been studied extensively and successfully, and due to the resemblance of their flux to background ratio with cosmic rays we draw gamma-ray Astronomy techniques such as significance measurements to study cosmic rays.

In gamma ray astronomy a positive result is when you have an excess amount of counts due to the existence of a source, and not due to background fluctuations. One must be really careful when evaluating a positive result. Over the years, many have worked on estimating the significance of a positive result, and it has been reported that a large number of positive results could easily be due to background fluctuations and thus their significance was overestimated [4]. Here we will follow the work of Li & Ma and use equation (9) [5] to calculate the significance of an assumed source:

$$S = \frac{N_s}{\widehat{\sigma}(N_s)} = \frac{N_{on} - \tau N_{off}}{\sqrt{\tau(N_{on} + N_{off})}} \tag{1}$$

They define the significance S as the photons that are coming from a supposed source (N_S) over its standard deviation $\widehat{\sigma}(N_S)$. As for the rest of the quantities, τ is defined as t_{on}/t_{off} where t_{on} is the time that the telescope points towards a supposed source, and counts N_{on} photons, and then, turns for background measurements for a time interval t_{off} and collects N_{off} photons. Now the background photons that are included in the N_{on} counts are $N_B = \tau N_{off}$, and the photons coming from the source are $N_S = N_{on} - N_B = N_{on} - \tau N_{off}$ [5]. It is also important to state that they also tested the precision of this formula by Monte Carlo Simulations.

Now let us assume that we are observing a source with flux $F = \frac{N_{on}}{At_{on}}$ over a uniform background of intensity $I = \frac{N_{off}}{A\pi\Delta\theta^2 t_{off}}$ where A is the telescope's effective area, and $\Delta\theta$ is the angular resolution. Then by solving for N_{on} and N_{off} and substituting in equation (1) we get

$$S = \sqrt{At_{on}}\frac{F - \pi I\Delta\theta^2}{\sqrt{\tau F + \pi I\Delta\theta^2}} \tag{2}$$

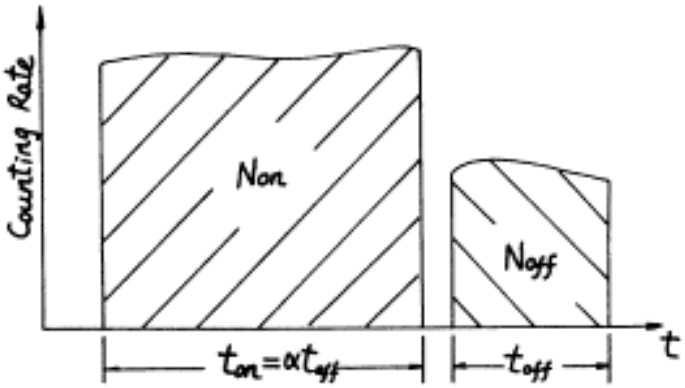

Figure 5: Picture taken from [5], representing a typical observation in gamma-ray Astronomy, where $\alpha = \tau$

Better angular resolution means smaller $\Delta\theta$. So from the equation above we see that if we manage to improve the telescope's angular resolution $\Delta\theta$, the fraction's numerator will increase while the fraction's denominator will decrease, meaning a total increase for the significance. But how much is this improvement?

If we assume that a source sent us -n- UHECRs, then on their way to Earth they will be deflected by the galactic magnetic field and so they will be observed scattered over a solid angle $\Delta\Omega(= \pi\Delta\theta^2)$. In this solid angle we might also have UHECRs coming from other background sources and so in our analysis we should consider some of the points to be them.

A bonus we get by effectively reconstructing the cosmic ray trajectories is that the scattered points will tend to cluster together closely, meaning that this solid angle will shrink. Chances are that a background source that was inside the solid angle will not happen to be in the exact same line of sight with the front source and so with the re-map, it will slightly stand out from the cluster, and that would in turn increase the significance.

2.6 Effectiveness Coefficient α (alpha)

Now let us connect the variable $\Delta\theta$ with the "effectiveness coefficient α (alpha)" from [6]. It can be seen in section 2.4 of [6] that after back-propagating each particle, due to errors, there is still a residual angle (ϕ_{res}) that separates the corrected position with the true position of the source as seen in the figure bellow, and it can be calculated.

Then, the initial angle between the recorded position on Earth and the true position of the source is also calculated (ϕ_{defl}). So now the effectiveness coefficient can be defined as

$$\alpha = \frac{\phi_{res}}{\phi_{defl}} \tag{3}$$

Thus, small values of α, correspond to a better correction. Of course for $\alpha > 1$, the residual angle is greater than the initial deflection angle, and so by back-propagating a cosmic ray through the Galaxy would have made things worse. As we improve the correction (meaning that progressively we have better accuracy for the magnetic field), the effectiveness

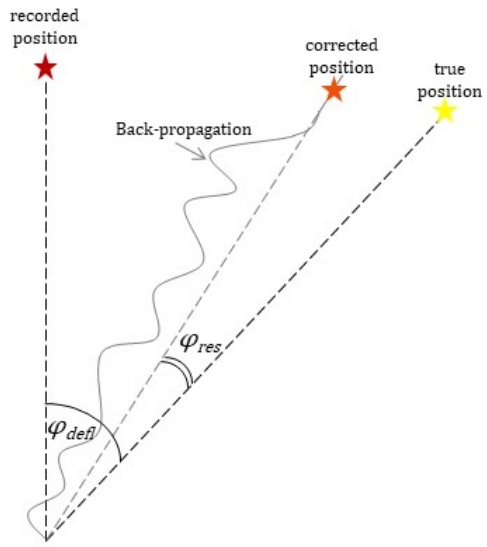

Figure 6

coefficient α gets smaller, and that is where we want to see significance levels going up. In this work we will focus on studying the relation between S and α.

3 Our work

3.1 The main idea/purpose

So let's assume that we have the magnetic tomography of our galaxy. Then, we can input the positions of the until-today recorded UHECRs in a code [6] that back-propagates their trajectory. At this point we would have a new map, where the points would have clustered towards their sources, and how much depends on our knowledge of the magnetic field, and their composition. We would also know the initial positions of these points and so what cluster they would make before the back propagation. That leaves us with before and after clusters, to whom we can apply Li & Ma statistics and measure how the significance of the detection of the supposed source (whose position is somewhere in the cluster) changed after this procedure. Of course we want to see how this significance ratio changes for different values of alpha. Then theoretically one could see depending on the desired significance one wants, what alpha is needed, and then in turn see [6] how good our knowledge of the magnetic field should be.

3.2 The data set

3.2.1 Real data

The data set we used in this work consists of 231 events recorded between 2004 and 2014 by the Pierre Auger Observatory. Their energies range from 50 to 127.1 EeV (1 EeV = 10^{18} eV) and due to the observatory's geographical location, the arrival directions have zenith angle up to 80 degrees [7] (meaning -90 to +45 in declination).

3.2.2 Mock data

Mock data is made-up data inserted into a software to simulate real data behavior in controlled ways. Specifically they can help in some of the following cases. Firstly, with the debugging because it is easier with many data to stress the code and find corner cases. Also we can simulate circumstances with a different number of data sets, and find possible errors that did not show up by the real data set, a) due to randomness or b) not yet with the calculations done so far.

Another case is when you don't have the real data yet but you write the processing software in advance. That could be when the experiment is expected to be performed in the near future, or such as in our case, the flux of UHECRs is so low (1 per km^2 per century) that we don't have enough data yet to have strong statistics. That is why we created a random and uniform data set with 800 supposed UHECRs. We assumed a uniform map (which would mean that the UHECRs are completely spread by the galactic magnetic field), because that would be the worst case compared to starting with a map, that has some slightly preferred positions, around which you would have small clustering.

3.3 Program Flow

In order to do the required calculations to implement our idea and study the relation between S and α , we constructed a numerical code. The code, created from scratch, produces all

the procedure described in more detail in the next steps. The program is used on the Pierre Auger Observatory data as well as the mock data.

(1) Define number of sources

(2) Pick the sources randomly, or set them by hand, or use most energetic of all as sources

(3) Find all distances

(4) Make clusters

(5) Drop points by finding dense centre and defining acceptable range. Make them background 1 component

(6) Define background 2 component randomly

(7) Re-locate points towards most energetic one

(8) Exposure time weight

(9) Count points in areas 1,2,3,4

(10) Calculate significances

(11) Iterate for many alpha

Now let us see these steps in more detail:

(1) This is a parameter defined at the beginning of the programme.

(2) Next, we choose the sources. When the data are not many and we can supervise the map, we can select them by hand based on excess of points in some areas. If this is not possible, or no preferred positions seem to exist then we can choose the sources randomly, or by some characteristic for example pick the ones with the highest energy. In our work, we chose them randomly. For that reason, we have to run the programme many times, in order to have results independent of randomness.

(3) Here we find for each point, its distance from all the others using equation (6) (see appendix A). This is needed for:

- Clustering. When we make the clusters we need to know the closest "neighbours" of our sources/seeds.
- Finding the centre of the densest area in a cluster. This is the point which determines which points will be dropped later depending if there are points beyond the acceptable range.
- Using the "acceptable range" parameter (see below).

(4) Here is where we do the clustering. After picking the sources, then each one of them picks its closest "neighbours", by picking in each round the next nearest point after checking a bitmap to see if that point is still available to pick.

(5) Acceptable range is the distance we consider to be reasonable, in order for 2 points to belong in the same cluster. So after we have found the point which is in the densest area of the cluster, then depending on the desired range, we drop the points that are further away, and make them extra background (background 1 component)

(6) In order to have all cases covered, we set some of the initial points as background. The percentage of this background is defined by a parameter. The points are then selected, randomly from our dataset.

(7) This is the part where we re-map the points. We choose to move them towards the most energetic one because that one will have been deflected less and thus it is more reliable. That point will not be moved (fixed point).For each point, if we assume that its distance with the fixed point was L, then what defines its new position is that the new distance between them will be $L' = \alpha L$.Note that we are dealing with cases where $\alpha < 1$and so $L' < L$ .That definition allows the moved point to be on a circle (see appendix A).Now we need to random pick the one coordinate of the moved point on that circle, and the second coordinate will be defined by the circle equation with the freedom of a random sign $\pm$ (see appendix A).

(8) Due to its geographic location, the Pierre Auger Observatory does not observe the whole sky uniformly and it also has a blind spot. Of course we need to take that into account. Since areas next to each other, will have almost the same exposure time, it's clear why the assumption $\tau = ton/toff \sim 1$ is accurate if "off area" is chosen to be next to "on area".

(9) The areas 1,2,3,4 refer to on, off areas, before and after re-mapping. Specifically we have:

1. on before
2. off before
3. on after
4. off after

So by counting the points/cosmic rays inside those areas, we get the desired quantities we need to use Li & Ma equation.

(10) Here from Li & Ma equation we calculate the significances S before, S after, and then finally our quantity of interest: S ratio.

(11) Last but not least we run the previous steps for different alphas in order to plot the calculated S ratios with them and see their dependence.

4 Results

4.1 Real data

In the plots that follow we firstly see what the map with the 231 recorded events by the Pierre Auger Observatory looks like before any calculations. Then, in the next figure, we see the map after randomly assigning the positions of the sources and the clustering been done as described above. In that same figure we can also see the points highlighted with the brown squares, which are the dense centres. Also there are grey and light grey points which are the background points from dropping outliers from clusters, and the extra random component respectively. Last but not least we see some points with black squares. These are, in each cluster, the most energetic Cosmic Rays, towards to whom the rest of the points will move.

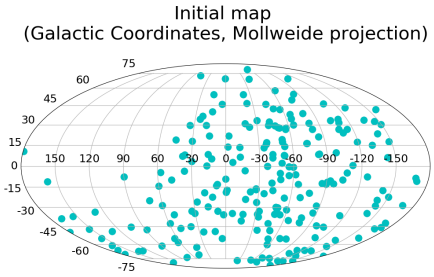

Figure 7a

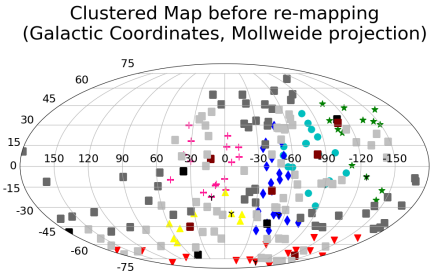

Figure 7b

Finally in the next 8 figures we can see how a reconstruction of the trajectories would look like, for various values of the parameter alpha. We see that even for high values of alpha, which translate to not so good knowledge of the 3-dimentional galactic magnetic field, we start to have some kind of clustering. Of course it becomes a lot more clear when alpha becomes 0.7 or smaller.

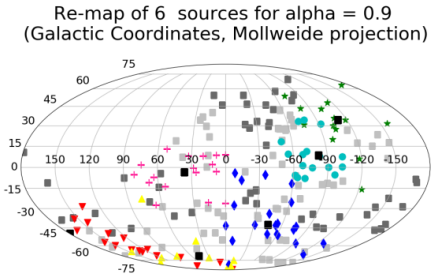

Figure 8a

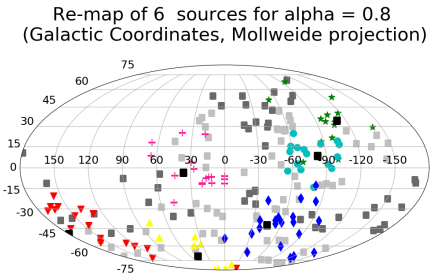

Figure 8b

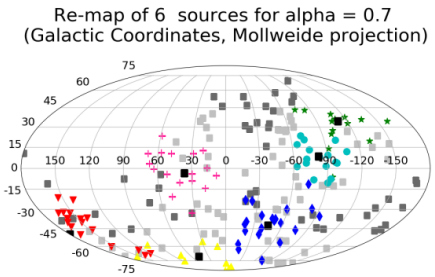

Figure 8c

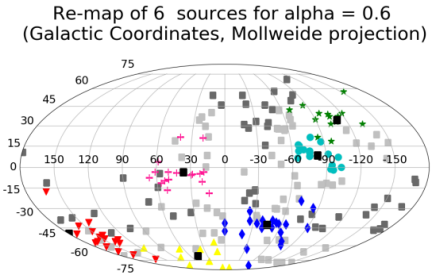

Figure 8d

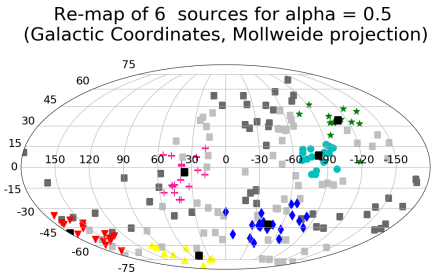

Figure 8e

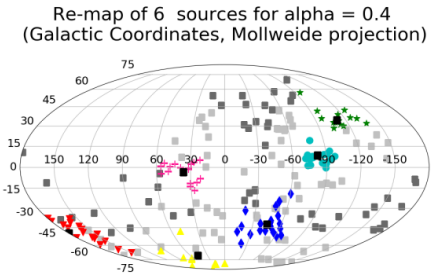

Figure 8f

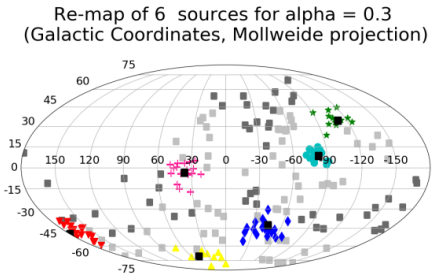

Figure 8g

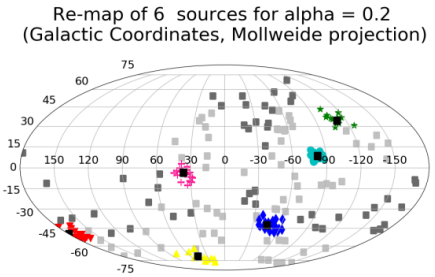

Figure 8h

In the next plot between the blue lines we see an example of what is considered to be the off area for the cluster shown in blue diamonds.

The code depends on random parameters, and so we run it several (50) times in order

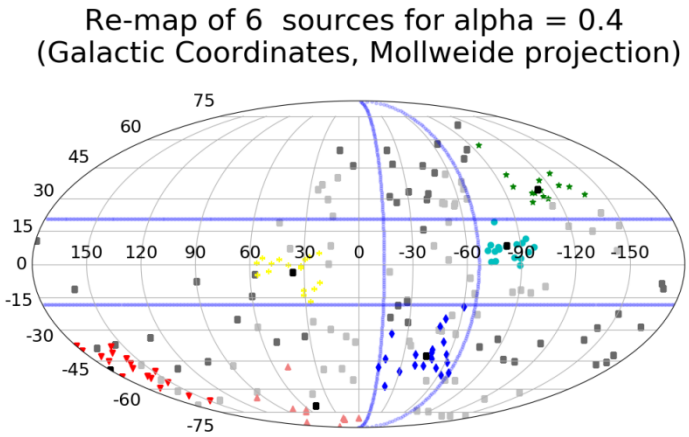

Figure 9

to make our results independent of that. Here we present some of the plots, including the extreme cases. On the x axis we have alpha and on the y axis we have the ratio of significance before over significance after the re-map. Of course we want that to be below 1 and so later we use the multiple-run data of all the rounds to count for each alpha, what percentage of the clusters improved their significance. Also we use that to calculate an average slope and error.

As we can see in the plots, we didn't run it for really small alpha, because the area of the cluster after re-mapping gets so small, that in the similar-size side off-area (taking into account the exposure time), you will not have 10 or above points, and so it is not correct/wise to use equation (1) to calculate the significance.

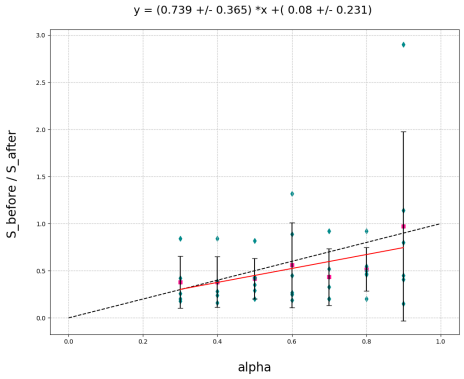

Figure 10a

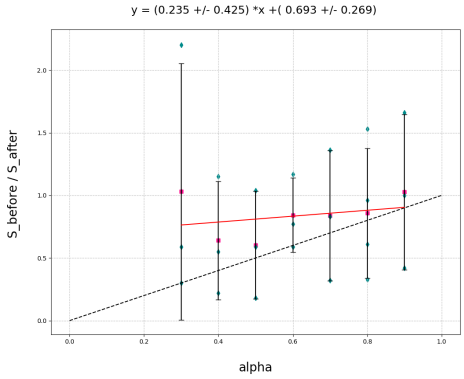

Figure 10b

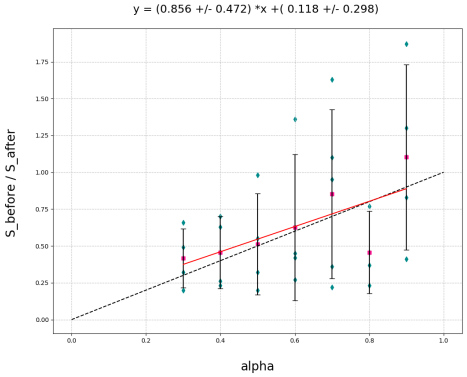

Figure 10c

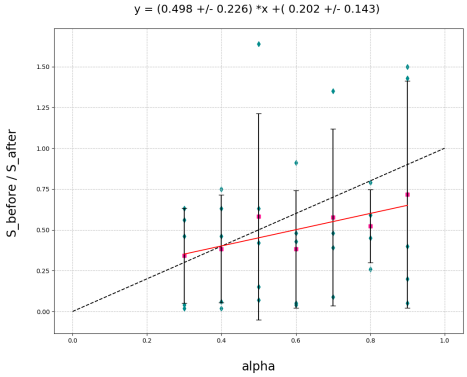

Figure 10d

Now as mentioned above, due the dependence of the results on randomness we did 50 realizations of the same process. So from that superset of data we calculated the average equation of the least squares fit, that being:

$$S\ ratio = (0.45 \pm 0.21)\alpha + (0.44 \pm 0.12) \tag{4}$$

Also from that superset of data we counted for each alpha, how many of the clusters actually give a higher level of significance. That calculation is presented in the chart that follows.

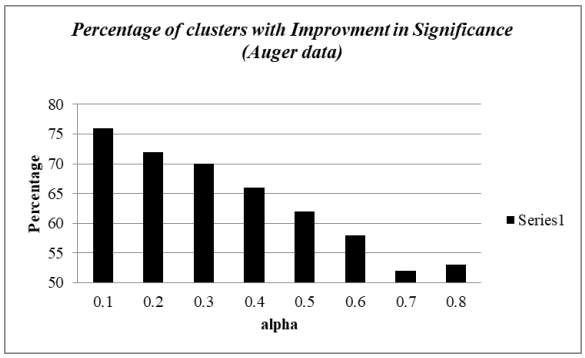

Figure 11

4.2 Mock data

Now let us see the same results, but for the mock data set.

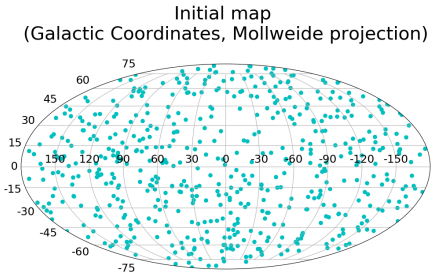

Figure 12a

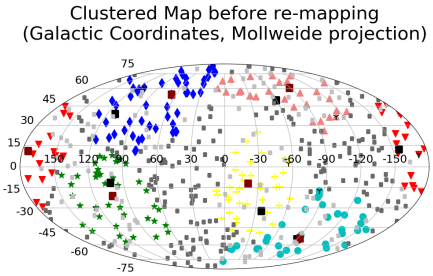

Figure 12b

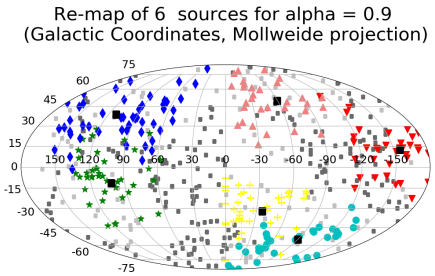

Figure 13a

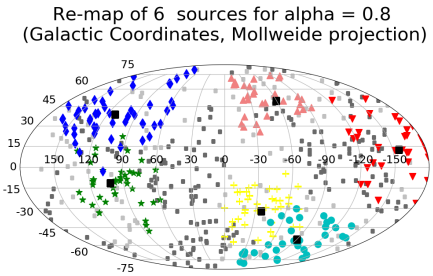

Figure 13b

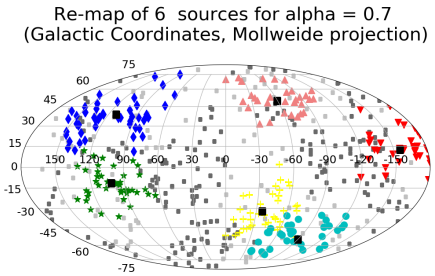

Figure 13c

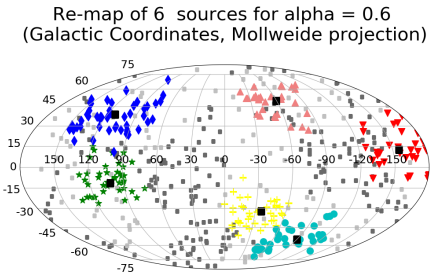

Figure 13d

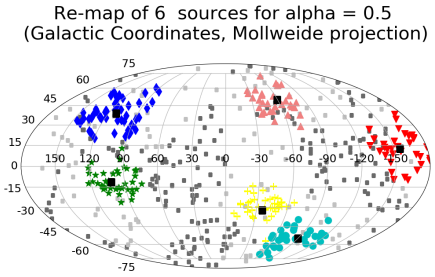

Figure 13e

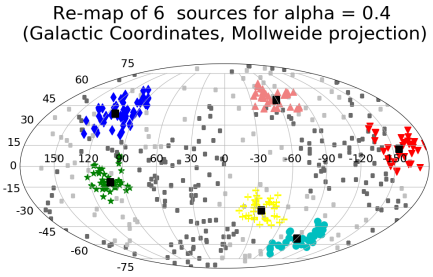

Figure 13f

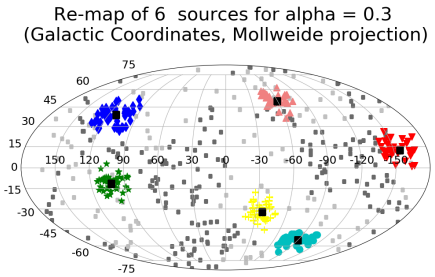

Figure 13g

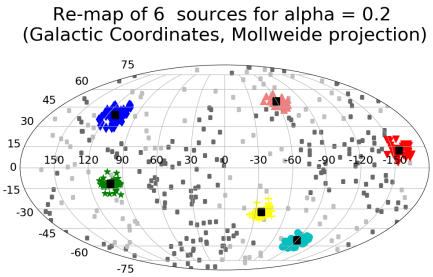

Figure 13h

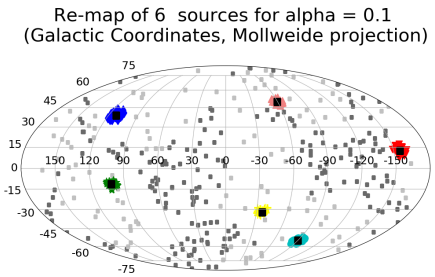

Figure 13i

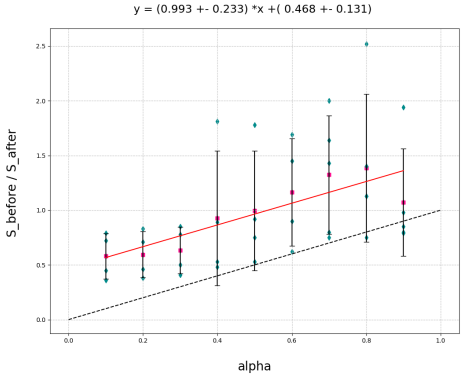

Figure 14a

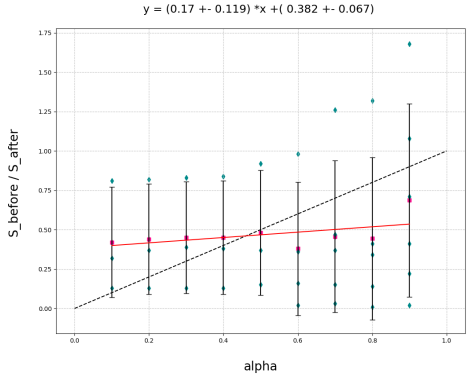

Figure 14b

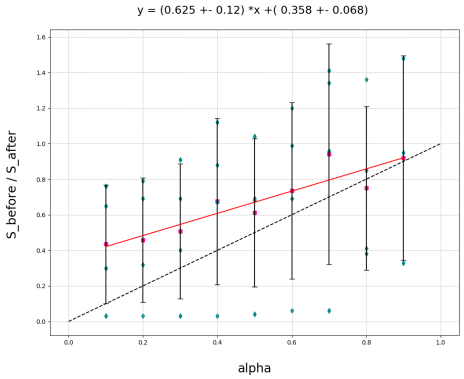

Figure 14c

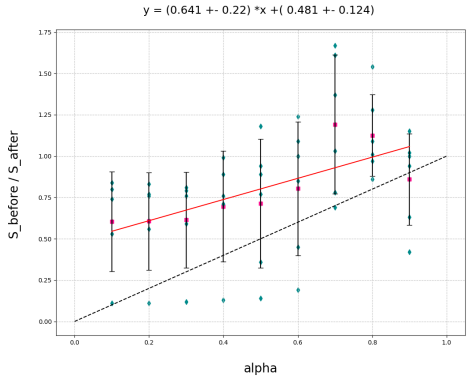

Figure 14d

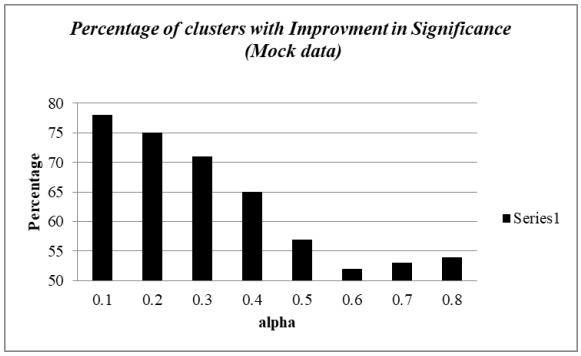

Figure 15

Here, after the 50 realizations we obtain for the mean least squares fit the following equation:

$$S\ ratio = (0.58 \pm 0.21)\alpha + (0.35 \pm 0.12) \tag{5}$$

5 Discussion

Comparing the results from the 2 data sets we see that we have a better correction, hence higher slope in the S ratios vs. alpha plot. It may seem not of a big quantitative difference, but it is qualitatively. That is because in the case of mock data, we are able to run the simulation for alpha reaching the value 0.1 without violating the Li & Ma requirement for Non or Noff being above 10, and so the second result is from a more reliable and wide range. In the figure that follows we can see the 2 results, combined with the expected one.

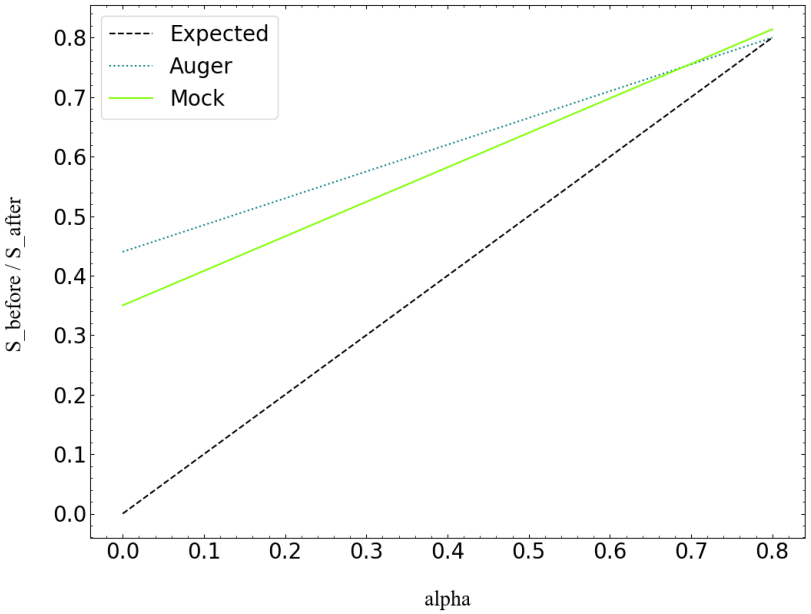

Figure 16

How can we know that there is not only 1 or 2 sources that produced all these points and so we would need a whole different approach in this simulation in order for it to be helpful? Well, we see an isotropic map produced by the Pierre Auger data. If we had very few sources, then we would see some anisotropy. That leads to our next point, that if we have at least few sources, then judging by the percentages chart , even for relatively high values of alpha, we can claim that there will be sources that could be detected since in all cases we have improved at least 50% of the clusters.

An example of the use of the equation obtained in S ratio plot is the following: assume that you reduce the deflection angles $\Delta\theta$ to half of their current values. Then $\alpha = 0.5$ and from the equation (3) you get $Sratio = 0.67$. That means that if you had a detection of a source with a 3σ initial significance, then after the correction it would become 4.5σ. And if you go further more in the correction, for $\alpha = 0.34$ and a 3σ initial significance, then you would get 5σ.

Li & Ma statistics require the counts (N_{on}, N_{off} quantities in equation (1)) to be above

10. So there are cases that this is quite hard to achieve due to the poor statistics in UHECRs. For example, when we have really small alpha, after re-mapping, the solid angle $\Delta\Omega$ shrinks so much that it is quite hard to have the counts in "off" area to be above 10. You can also run into this (not enough points) problem when you want to have many UHECR sources in the simulation, so you tend to run out of points even before re-mapping. Specifically the extreme case would be to have n/10 sources, where n is the total number of events.

Bad outcomes can also be encountered by not representative counts. A case for example is when we are counting the "off" points of a supposed source (A), and in the area we are looking happens to be another source (B). In that case, we are counting B source's "on" points to be A source's background, and that in turn will ruin our estimation of significance despite the fact that we decreased the solid angle where A source location is.

6 Future Work

One thing that would be reasonable to improve in our analysis is the calculation of the background component. The way it is calculated now, is dependent of the parameters of the code. Firstly, the most energetic points in each cluster define the after-positions of the clusters. Also, the acceptable range as well as the background percentage define the number of background points, and that in turn combined with the previous, define the positioning between them and the clusters. That dependence should be avoided by introducing a uniform background calculated completely independently of our simulation. This background should be of the form counts per area.

One thing that has not been calculated in this work is the probability of having a "fake" cluster. That could happen either by having large errors, or by moving the points wrong due to the freedom we have around the supposed source. That means that we could move the point to the other end of the source that it was before ("over-correcting").

We could also improve this simulation, by using more sophisticated algorithms for clustering, or trying to use 2-point correlation function techniques. Lastly, since now we have a code to work on, we could try various alternative approaches of this problem (like having only one dominant source) by simulating with different values of the parameters of the code, so we could possibly extract more patterns and conclusions.

A Math

Let's assume that we have 2 points, with coordinates (x, y, z) and (x', y', z') in the same distance. If the galactic longitude (l) varies from -180 to +180 degrees, the galactic latitude (b) varies from -90 to +90 degrees and we are at the center, then the angular distance (ψ) between them given by the inner product is:

$$v_1 v_2 = R^2[\cos(b)\cos(b')cos(l-l') + \sin(b)\sin(b')] \equiv R^2 A$$

$$\text{and } v_1 v_2 = R^2 cos(\psi) \Rightarrow$$

$$\psi = \arccos(A) \tag{6}$$

In the figure that follows, we can see the re-location of the points. In the centre, with a star is the fixed point, and around it, it has the rest points of the cluster. The dashed circle line is the possible new locations of the point that is now at distance L.

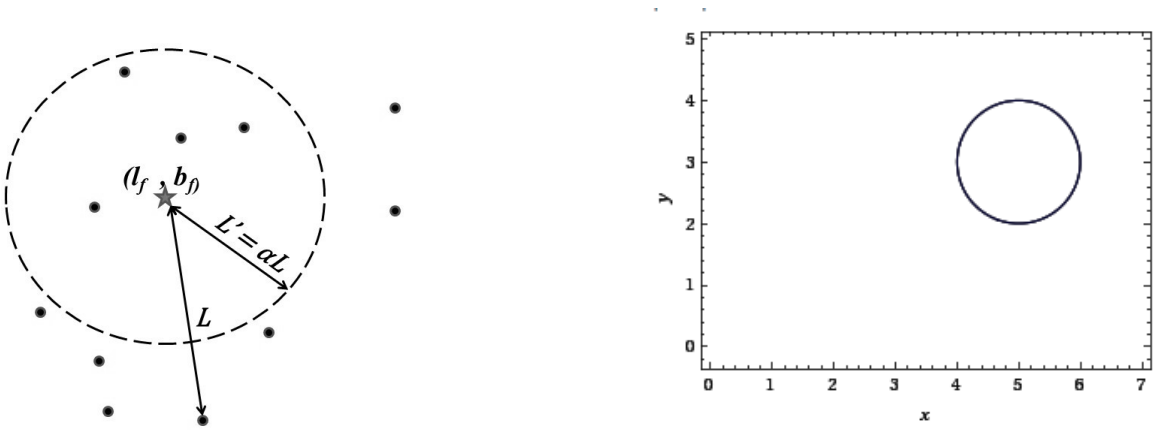

The way we define the new position on that circle is the following: Imagine this simple 2-dimensional example where the circle equation is$(x-5)^2 + (y-3)^2 = 1$.Then if we want a random point on that circle, we have to choose a random x in the [4, 6] interval, and then y will be defined by the circle equation with the freedom of a $\pm$ sign.

In our work, we follow the same logic on the surface of the sphere defined by our points, (That surface is created because we only know their line of sight position and so due to lack of knowledge in their distance we assume them all to be in radius = 1) with the circle equation being:

$$(x-x_f)^2 + (y-y_f)^2 + (z-z_f)^2 = R^2 \Rightarrow$$

$$(\cos(b_j)cos(l_j) - \cos(\alpha\psi)\cos(b_f)cos(l_f))^2 + (\cos(b_j)sin(l_j) - \cos(\alpha\psi)\cos(b_f)sin(l_f))^2 +$$

$$(\sin(b_j) - \cos(\alpha\psi)\sin(b_f))^2 = (\sin(\alpha\psi))^2 \tag{7}$$

Where α is the effectiveness coefficient, ψ is the initial angular distance between the 2 points, f denotes the coordinates of the fixed points, and j refers to the new coordinates of each point that will be moved. In the next figure we can see this representation, and all the inferred distances.

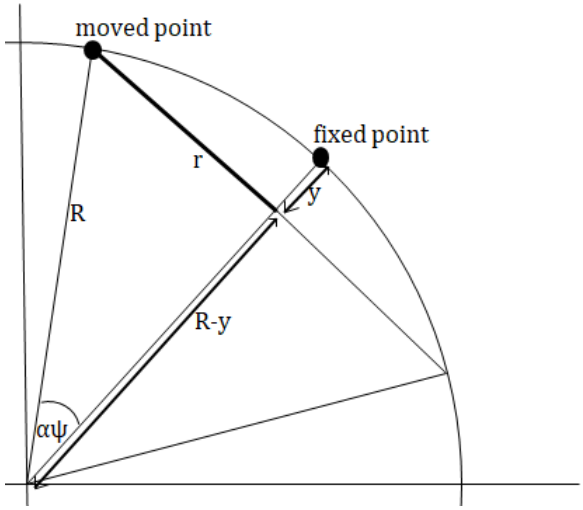

Here we considered a sphere with very large radius to be cut by a plane defined by the distance of the 2 points. We see that the desired circle has a radius $r = R\sin(\alpha\psi)$, and the center has angular coordinates same with the fixed point, but its distance is $R - y = R\cos(\alpha\psi)$.

B Pierre Auger Observatory Data

List of the 231 events with energies above 50 EeV and $\theta < 80°$. The columns are: year, day, zenith angle , energy (EeV) , right ascension, declination, Galactic longitude and latitude.

YYYY	DDD	Theta	Energy	RA	dec	Lon	Lat
2004	125	47.7	62.2	267.2	-11.4	15.5	8.4
2004	142	59.2	84.7	199.7	-34.9	-50.8	27.7
2004	177	71.5	54.6	12.7	-56.6	-56.9	-60.5
2004	239	58.3	54.0	32.7	-85.0	-59.1	-31.8
2004	282	26.3	58.6	208.1	-60.1	-49.5	1.9
2004	339	44.6	78.2	268.4	-61.0	-27.6	-16.9
2004	343	23.3	58.2	224.7	-44.0	-34.1	13.1
2005	50	67.5	60.2	29.0	-14.0	174.9	-70.0
2005	54	34.9	71.2	17.5	-37.8	-76.0	-78.6
2005	63	54.4	71.9	331.2	-1.3	58.7	-42.4
2005	81	17.1	52.1	199.1	-48.5	-52.8	14.1
2005	186	57.5	108.2	45.6	-1.7	179.5	-49.6
2005	233	65.4	61.9	278.4	-1.3	29.7	3.4
2005	295	15.3	54.9	333.0	-38.1	4.4	-55.0
2005	306	14.2	74.9	114.8	-42.8	-103.9	-10.0
2005	347	65.6	77.5	18.3	29.2	128.6	-33.4
2006	5	30.9	78.2	18.9	-4.7	138.3	-66.8
2006	35	30.8	72.2	53.6	-7.8	-165.9	-46.9
2006	55	37.9	52.8	267.6	-60.6	-27.5	-16.4
2006	64	66.6	64.8	275.2	-57.2	-22.6	-18.6
2006	81	34.0	69.5	201.1	-55.3	-52.3	7.3
2006	100	33.7	54.7	28.8	-16.4	-179.9	-71.8
2006	118	57.3	56.3	322.5	-2.0	51.6	-35.6
2006	126	65.2	82.0	299.0	19.4	57.6	-4.7
2006	142	22.6	64.3	121.8	-52.5	-93.0	-10.7
2006	160	76.5	60.7	52.7	-43.4	-109.6	-54.1
2006	185	58.8	89.0	349.9	9.3	88.4	-47.3
2006	263	49.9	53.0	82.1	14.6	-169.9	-10.9
2006	284	54.5	54.0	142.3	-13.1	-114.3	26.6
2006	296	53.9	67.7	53.0	-4.5	-170.5	-45.6
2006	299	26.0	59.5	200.9	-45.3	-51.2	17.2
2006	350	17.6	60.0	305.6	-46.3	-6.4	-34.5
2007	9	54.0	53.8	321.0	8.1	60.4	-28.7
2007	13	14.2	127.1	192.8	-21.2	-57.1	41.7
2007	14	55.9	52.2	192.6	17.2	-58.4	80.1
2007	69	30.4	60.0	200.2	-43.4	-51.4	19.2
2007	84	17.5	60.8	143.4	-18.1	-109.4	24.1
2007	106	49.8	70.3	17.5	13.6	129.8	-49.0

YYYY	DDD	Theta	Energy	RA	dec	Lon	Lat
2007	145	24.0	68.4	47.5	-12.8	-164.0	-54.5
2007	161	41.9	53.6	137.3	6.2	-135.9	33.4
2007	166	79.6	54.9	245.8	8.5	22.9	36.7
2007	186	44.9	61.5	219.5	-53.9	-41.7	5.8
2007	193	17.9	79.7	325.5	-33.4	12.2	-49.0
2007	203	55.3	57.0	265.9	5.9	30.5	17.8
2007	205	76.5	61.9	195.5	-63.4	-55.9	-0.6
2007	221	35.5	67.8	212.8	-3.1	-21.6	54.2
2007	227	33.6	60.7	192.5	-35.3	-57.3	27.5
2007	234	33.3	68.1	185.3	-27.9	-65.2	34.5
2007	235	42.6	60.8	105.9	-22.9	-125.2	-7.7
2007	295	21.1	65.9	325.7	-15.5	37.8	-44.8
2007	295	56.5	55.8	39.2	19.4	154.4	-36.9
2007	314	76.7	52.5	59.6	38.3	158.5	-11.3
2007	339	68.2	54.0	250.3	1.8	18.5	29.5
2007	343	30.9	82.4	81.6	-7.4	-150.1	-22.3
2007	345	51.6	72.7	315.3	-53.8	-16.0	-40.5
2008	10	77.1	80.2	271.1	19.0	45.2	18.7
2008	13	16.8	64.2	252.7	-22.7	-1.9	13.7
2008	18	50.2	111.8	352.6	-20.8	47.5	-70.5
2008	36	28.3	65.3	187.5	-63.5	-59.5	-0.7
2008	48	76.9	60.4	19.8	-25.5	-160.1	-83.6
2008	49	50.7	56.0	64.1	-52.7	-98.5	-44.4
2008	51	20.7	53.3	202.0	-54.9	-51.8	7.6
2008	52	31.7	56.2	82.8	-15.8	-141.2	-24.7
2008	72	4.4	52.4	184.4	-32.4	-65.2	30.0
2008	87	38.9	73.1	220.6	-42.8	-36.3	15.5
2008	118	36.2	62.9	110.2	-0.9	-142.9	6.1
2008	142	43.4	56.7	199.4	6.6	-39.0	68.5
2008	184	53.7	55.7	33.0	11.0	152.8	-47.2
2008	192	20.2	55.1	306.5	-55.1	-17.1	-35.3
2008	205	53.1	56.7	358.9	15.5	103.6	-45.2
2008	250	68.8	52.0	67.7	4.0	-168.7	-28.6
2008	264	44.4	89.3	116.0	-50.6	-96.4	-12.9
2008	266	59.0	61.2	339.4	-63.3	-35.4	-47.8
2008	268	49.8	118.3	287.7	1.5	36.5	-3.6
2008	282	29.0	58.1	202.2	-16.1	-44.2	45.9
2008	296	42.8	64.7	15.6	-17.1	137.9	-79.6
2008	322	28.4	62.2	25.0	-61.4	-67.1	-54.8
2008	328	47.2	63.1	126.4	5.3	-140.8	23.4
2008	329	47.9	66.9	28.9	-2.7	157.9	-61.2
2008	331	50.7	52.6	304.4	-26.2	16.7	-29.6
2008	337	30.8	65.8	275.2	-14.4	16.7	0.1
2008	355	71.7	71.1	196.1	-69.7	-55.9	-6.9

YYYY	DDD	Theta	Energy	RA	dec	Lon	Lat
2008	362	31.5	74.0	209.6	-31.3	-40.7	29.4
2009	7	59.2	61.0	286.3	-37.8	-0.6	-18.7
2009	30	32.3	66.2	303.9	-16.5	26.8	-25.8
2009	32	56.2	70.3	0.0	-15.4	75.0	-73.2
2009	35	52.8	57.7	227.0	-85.2	-54.2	-23.1
2009	39	42.4	64.1	147.2	-18.3	-106.5	26.6
2009	47	20.7	52.9	78.3	-16.0	-142.9	-28.8
2009	51	6.9	66.7	203.4	-33.0	-47.0	29.1
2009	73	37.0	72.5	193.8	-36.4	-56.2	26.5
2009	78	27.2	74.4	122.7	-54.7	-90.7	-11.4
2009	78	8.2	59.0	26.7	-29.1	-134.5	-77.6
2009	80	18.4	65.8	251.4	-35.8	-13.0	6.3
2009	80	44.4	63.8	170.1	-27.4	-80.8	31.3
2009	83	68.6	56.2	249.1	9.1	25.3	34.1
2009	140	27.2	55.1	330.8	-8.9	49.5	-46.3
2009	160	40.9	52.8	43.9	-25.4	-143.4	-62.2
2009	162	78.2	70.5	39.4	-34.5	-122.6	-66.1
2009	163	41.2	71.9	23.3	-40.2	-87.9	-74.3
2009	172	9.7	65.8	276.1	-33.4	0.1	-9.4
2009	191	26.9	59.5	294.5	-20.5	19.1	-19.2
2009	197	51.7	52.2	129.4	15.2	-149.5	30.2
2009	202	60.8	63.6	358.2	-2.8	90.4	-61.9
2009	212	52.7	55.3	122.5	-78.5	-68.8	-22.8
2009	219	40.1	53.2	29.4	-8.6	166.2	-65.8
2009	219	59.7	58.3	304.3	-81.9	-48.3	-29.8
2009	237	78.4	70.0	325.8	42.8	90.1	-7.8
2009	250	70.7	52.3	212.7	29.9	46.8	72.3
2009	262	22.4	58.7	50.1	-25.9	-140.5	-56.7
2009	274	79.4	82.3	287.7	-64.9	-28.9	-26.4
2009	281	75.5	75.3	256.7	14.0	34.2	29.4
2009	282	47.2	60.8	47.6	11.5	168.6	-38.7
2009	288	34.2	58.6	217.9	-51.5	-41.6	8.4
2009	304	30.1	55.6	177.7	-5.0	-83.8	54.7
2009	335	64.2	52.5	171.3	-43.8	-73.1	16.4
2010	24	73.6	54.3	97.2	34.3	179.7	10.6
2010	45	70.0	61.5	174.7	-21.2	-78.9	38.6
2010	50	71.7	64.5	227.9	-21.5	-18.6	30.7
2010	52	52.1	72.9	258.1	-44.9	-17.0	-3.3
2010	72	43.3	66.9	278.8	7.9	38.2	7.2
2010	121	43.6	82.0	122.7	-70.7	-76.3	-19.3
2010	148	52.2	74.8	89.2	-12.0	-142.2	-17.5
2010	182	15.4	54.7	197.8	-20.0	-50.7	42.6
2010	193	69.6	58.4	149.2	5.5	-127.5	43.2
2010	194	70.9	53.8	277.2	6.7	36.4	8.1

YYYY	DDD	Theta	Energy	RA	dec	Lon	Lat
2010	196	73.2	52.3	303.7	-68.1	-32.6	-32.8
2010	204	38.7	53.2	180.5	-11.5	-75.9	49.6
2010	205	47.4	53.5	315.8	-82.1	-49.3	-31.2
2010	223	39.0	56.1	250.2	-73.6	-42.6	-17.5
2010	224	62.3	65.2	284.7	-28.2	8.1	-13.9
2010	226	53.8	75.6	324.5	17.9	71.2	-25.0
2010	235	32.0	60.3	216.1	-66.5	-48.0	-5.3
2010	238	12.4	69.6	226.4	-25.7	-22.6	28.1
2010	239	66.7	58.4	312.9	-14.2	33.1	-33.0
2010	256	73.8	76.1	131.9	-15.5	-118.9	17.1
2010	277	31.1	73.7	12.3	-40.7	-55.3	-76.5
2010	284	48.6	89.1	218.8	-70.8	-48.7	-9.7
2010	295	27.8	58.0	8.4	-61.5	-53.3	-55.5
2010	310	45.4	53.1	118.1	8.5	-147.9	17.4
2010	311	58.4	70.5	64.2	-46.5	-107.2	-45.5
2010	319	11.4	55.0	118.6	-37.4	-107.2	-4.8
2010	320	29.0	54.3	80.2	-64.1	-86.2	-34.1
2010	320	5.1	68.7	121.1	-30.6	-111.9	0.4
2010	342	40.5	54.6	170.9	-43.7	-73.4	16.4
2010	347	24.6	54.9	231.9	-56.6	-36.7	0.0
2010	348	33.8	54.4	179.7	-68.6	-61.9	-6.2
2010	364	22.2	68.0	167.0	-31.2	-81.8	26.6
2011	19	43.8	69.4	268.5	-15.7	12.4	5.1
2011	26	25.0	100.1	150.1	-10.3	-110.9	34.1
2011	35	71.5	54.0	185.4	-24.6	-65.6	37.8
2011	38	33.8	58.2	33.4	-31.7	-127.8	-71.5
2011	41	59.2	52.0	125.5	-59.2	-86.0	-12.5
2011	45	25.5	62.7	215.5	-10.1	-23.5	46.8
2011	49	39.3	60.3	239.4	3.9	13.8	39.9
2011	75	60.5	71.1	230.3	1.5	3.8	45.9
2011	86	59.4	56.2	160.3	-3.1	-108.3	46.4
2011	106	78.2	81.4	308.8	16.1	59.9	-14.3
2011	111	65.6	69.7	30.3	3.8	154.2	-54.8
2011	113	71.5	54.8	295.1	-27.6	12.2	-22.3
2011	119	53.0	67.3	255.4	-5.1	14.8	21.6
2011	120	49.8	72.1	84.9	14.4	-168.3	-8.7
2011	132	10.6	56.8	39.5	-29.9	-134.1	-66.5
2011	136	54.1	64.9	333.8	-79.2	-48.7	-35.3
2011	162	72.4	55.9	132.8	12.9	-145.5	32.4
2011	203	29.9	77.9	120.8	-56.3	-89.8	-13.2
2011	207	65.0	56.4	344.5	-19.9	42.3	-63.1
2011	215	34.5	68.3	245.4	-18.2	-2.8	21.8
2011	221	2.9	70.8	139.8	-35.8	-98.2	9.6
2011	240	46.5	58.8	219.1	-41.9	-36.9	16.8

YYYY	DDD	Theta	Energy	RA	dec	Lon	Lat
2011	252	24.5	80.9	283.7	-28.6	7.4	-13.2
2011	294	31.8	75.6	77.2	-41.0	-114.4	-36.1
2011	307	40.7	52.4	313.5	-16.6	30.7	-34.4
2011	309	38.8	63.3	26.1	-32.2	-120.2	-77.4
2011	316	31.0	70.2	4.6	-37.9	-26.2	-77.2
2011	318	36.7	57.2	148.8	-13.0	-109.6	31.4
2011	360	36.1	67.4	305.5	-34.5	7.6	-32.7
2011	361	47.6	92.8	343.4	-71.6	-44.9	-42.6
2011	364	51.7	64.8	207.1	-29.1	-42.4	32.1
2012	12	31.8	62.4	15.3	-3.6	129.0	-66.3
2012	52	23.8	66.1	33.2	-59.0	-75.3	-55.2
2012	81	47.3	99.0	309.4	-66.8	-31.5	-35.2
2012	103	67.5	70.4	154.0	-46.3	-83.1	8.6
2012	109	25.9	62.6	37.8	-39.5	-110.0	-65.9
2012	132	62.3	58.5	189.0	-5.1	-64.1	57.6
2012	154	65.8	58.7	37.0	-75.8	-64.6	-39.9
2012	155	64.3	60.0	245.4	-30.9	-12.7	13.3
2012	162	58.5	83.8	26.8	-24.8	-154.6	-77.3
2012	183	59.8	61.8	259.8	-32.7	-6.2	2.7
2012	189	31.4	61.1	18.7	-42.5	-72.9	-73.9
2012	193	65.5	54.4	342.9	-6.5	63.4	-54.8
2012	206	61.6	56.8	310.6	-83.1	-50.0	-30.2
2012	211	50.0	58.7	177.2	12.5	-105.1	69.3
2012	301	38.5	53.3	56.3	-3.2	-169.2	-42.1
2012	332	48.1	71.1	227.6	11.9	14.7	54.0
2013	11	17.0	55.7	217.1	-24.5	-30.5	33.3
2013	27	26.5	62.7	200.9	-34.6	-49.6	27.8
2013	27	47.6	70.7	56.6	-67.8	-77.6	-41.7
2013	31	67.3	53.2	314.9	-67.3	-32.8	-37.1
2013	36	74.7	73.6	267.5	-68.3	-34.8	-19.7
2013	52	60.7	71.9	73.7	-20.5	-139.8	-34.4
2013	70	41.9	53.9	154.3	-15.8	-102.7	33.1
2013	119	61.5	62.1	138.6	26.1	-158.8	41.9
2013	132	59.3	57.3	357.0	-81.1	-54.1	-35.7
2013	134	44.9	85.3	123.4	-6.2	-131.7	15.1
2013	144	49.8	54.3	33.3	-39.0	-107.2	-69.2
2013	163	44.6	52.2	0.4	-68.1	-50.1	-48.3
2013	175	50.6	58.9	211.1	15.0	1.0	69.1
2013	190	57.3	68.8	64.7	-70.1	-77.0	-38.0
2013	191	8.8	67.3	308.1	-39.5	2.1	-35.7
2013	222	63.4	61.5	240.3	-68.9	-41.3	-12.1
2013	224	47.9	63.4	345.4	-9.0	62.7	-58.3
2013	247	54.7	84.8	154.6	-46.9	-82.4	8.3
2013	249	30.0	55.5	160.4	-34.8	-85.2	20.9

YYYY	DDD	Theta	Energy	RA	dec	Lon	Lat
2013	249	55.0	65.4	92.1	-64.1	-86.4	-28.9
2013	281	65.1	58.5	327.5	-25.1	25.3	-49.4
2013	297	39.0	73.0	163.8	-74.1	-64.9	-13.1
2013	302	49.4	54.6	298.7	8.8	48.2	-9.8
2013	319	62.0	54.4	284.5	-37.6	-1.0	-17.3
2013	320	22.2	52.9	286.8	-55.0	-18.3	-24.1
2013	329	29.2	63.6	182.3	-14.3	-72.3	47.3
2013	332	31.1	65.2	241.6	-53.5	-30.5	-1.0
2013	352	51.4	72.5	91.4	-60.6	-90.4	-28.9
2013	364	60.2	53.2	198.8	-63.9	-54.5	-1.2
2014	8	57.9	60.0	72.8	-73.5	-74.4	-34.3
2014	30	60.8	74.5	189.9	-32.7	-60.0	30.1
2014	32	12.8	54.6	186.7	-24.9	-64.1	37.6
2014	49	41.7	54.9	2.3	-49.2	-39.7	-66.4
2014	59	25.9	60.2	239.5	-49.2	-28.7	3.0
2014	64	66.7	63.6	45.2	-65.8	-75.6	-46.4
2014	65	58.5	118.3	340.6	12.0	80.1	-39.9

References

[1] http://www.pasiphae.science

[2] arXiv:1710.09478 Highlights from the Pierre Auger Observatory (ICRC17)

[3] arXiv:1503.06961 Recent Results from Telescope Array

[4] doi: 10.1038/241376a0 Application of Statistics to Results in Gamma Ray Astronomy

[5] doi: 10.1086/161295 Analysis methods for results in gamma-ray astronomy

[6] arXiv:1802.03409 Deflections of ultra-high energy cosmic rays by the Milky Way magnetic field: how well can they be corrected?

[7] doi: 10.1088/0004-637X/804/1/15 Searches for anisotropies in the arrival directions of the highest energy cosmic rays detected by the Pierre Auger observatory.